

# Experimental Investigation of Aerodynamic Instability of Iced Bridge Cable Sections

**Koss, Holger; Lund, Mia Schou Møller**

*Published in:*
Proceedings of the 6th European and African Wind Engineering Conference

*Publication date:*
2013

*6th European and African Conference on Wind Engineering*
*7-11 July 2013, Robinson College, Cambridge, UK*

# Experimental Investigation of Aerodynamic Instability of Iced Bridge Cable Sections

Holger Hundborg Koss[1] , Mia Schou Møller Lund[1]

[1]Department of Civil Engineering, Technical University of Denmark, 2800 Lyngby, Denmark.

hko@byg.dtu.dk ; msml@byg.dtu.dk

**Abstract**

The accretion of ice on structural bridge cables changes the aerodynamic conditions of the surface and influences hence the acting wind load process. Full-scale monitoring indicates that light precipitation at moderate low temperatures between zero and -5°C may lead to large amplitude vibrations of bridge cables under wind action. This paper describes the experimental simulation of ice accretion on a real bridge cable sheet HDPE tube segment (diameter 160mm) and its effect on the aerodynamic load. Furthermore, aerodynamic instability will be estimated with quasi-steady theory using the determined load coefficients and experimental simulation on a 1DOF elastically suspended cable section.

## 1 Introduction

In recent years the relevance of ice accretion for wind-induced vibration of structural bridge cables has been recognised. Full-scale monitoring indicates that ice accretion from light precipitation at moderate low temperatures between zero and -5°C may lead to large amplitude vibrations of bridge cables under wind action. For the prediction of aerodynamic instability in connection to ice accretion existing quasi-steady models have been expanded to include beside load contributions from drag and lift also the effect of torsion (Gjelstrup *et al.*, 2008). A fundamental aspect in studying the influence of ice accretion on aerodynamic loading and structural response is the shape and surface texture of the ice layer. Literature reports usually the average ice contour line and even modern numerical simulation tools (Fu *et al.*, 2006) do not reflect the surface roughness of the ice layer. Additionally, the reported studies refer, either partially or entirely, to boundary condition outside the target range considered for bridge cables (Georgakis *et al.*, 2009). To understand the icing process, surface roughness characteristics and structure occurring at moderate low temperatures studies on smaller circular metal cylinders (diameter 38.1 and 89mm) have been conducted in the Altitude Icing Wind Tunnel at the National Research Council (NRC) in Ottawa, Canada (Koss *et al.*, 2011).

It became clear that for accurate modelling the influence of ice accretion on the aerodynamic load and response process full-size simulation will be required. The construction of a special Climatic Wind Tunnel was started in 2008 allowing tests on prototype bridge cable sections under variable flow and climatic conditions, in particular conditions related to *low-altitude atmospheric icing* (Georgakis *et al.*, 2009). The tests allow measuring the development of the aerodynamic forces during the accretion process, studying the load of static iced cables for variable incident flows and observe the structural response with a special free vibration rig. First results on ice accretion and static load coefficients have been published by Koss and Matteoni in 2011.

This paper will present the results from tests studying the aerodynamic drag and lift as a function of axial rotation of the iced cable and of the Reynolds number. The tests were performed on an original bridge cable sheet, a 160mm diameter HDPE tube segment mounted horizontally in the centre of the wind tunnel test section with flow normal to tube axis (Figure 1). The risk of aerodynamic instability is assessed by applying quasi-steady theory, in this case by the Den Hartog instability criterion. Selected configuration indicating instability will be tested in a dynamic experimental setup allowing free cross-flow vibration of the cable segment. In the following, the details of the test arrangement are introduced and briefly discussed.

## 2 Experimental Setup

The technical details of the Climatic Wind Tunnel (CWT) facility are described by Georgakis *et al.* (2009). The main technical specifications are: 5m long test chamber with a cross-section of 2 x 2m, maximum airspeed $u_{max}$ = 32m/s, lowest along-wind turbulence intensity is $I_{u,min}$ = 0.6%. The lowest long-term average temperature at full speed is -4.5°C. The blockage ration for a 160mm diameter cable segment is about 8%.

Horizontally mounted 15 nozzle spray bar operating in the settling chamber.

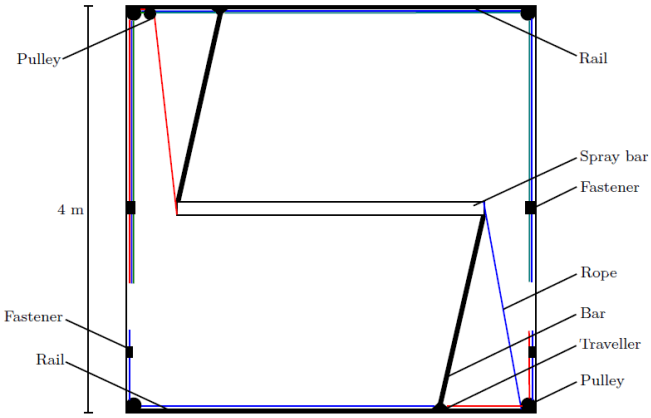


Spray bar supporting system consisting of pin-jointed arms and tension ropes.

Figure 1: Spray system design consisting of remote controlled spray bar (*left*) and variable support system allowing free rotation of the spray bay to accommodate inclined cable testing conditions (*right*).

The innovative part of the experimental setup for simulating low altitude atmospheric icing or low altitude in-cloud icing, respectively, is the rotatable spray bar. Differing from the design in other icing wind tunnels (see Oleskiw *et al.*, 2001, for NRC design) the CWT spray system generates cloud-like spray only in the cable-wind plane. In order to accommodate the different orientation of inclined cables the spray bar can freely be rotated. Figure 1 shows to the right a sketch with the main elements of the support system. The arm articulation points and rope pulley locations are steplessly adjustable. Results from icing tests in the above described CWT setup on a vertical cable section are reported in parallel papers by Demartino *et al.* (2013a) and on an inclined cable in Demartino *et al.* (2013b). Inside the spray bar the water supply tubes and spray nozzles are heated, air and water pressure are monitored by integrated sensors close to the nozzles and the water supply can be switched off by remote controlled valves. The spray nozzles are off-the-shelf products allowing producing droplets in the size range (median volume diameter, *MVD*) between 10 and 80µm depending on the air/water pressure ratio.

## 3 Test Cases and Ice Accretion

The study is based on two different climatic conditions characterised by wet and dry ice accretion. Table 1 summarises the boundary conditions for the study.

Table 1: Specifications of the climatic conditions in the study.

| ID | wind speed [$m/s$] | mean air temperature [$°C$] | LWC target [$g/m^3$] | MVD [$\mu m$] | accretion time [$min$] | ice mass [$kg/m$] | ice thickness mean (a) [$mm$] | ice thickness max (b) [$mm$] |
|---|---|---|---|---|---|---|---|---|
| H1 | 11 | -6.3 | 0.4 | 0.2 | 60 | 2.2 | 20.0 | 28.0 |
| H2 | 11 | -3.2 | 0.4 | 0.2 | 60 | 1.1 | 4.6 | 11.6 |

Note: LWC = liquid water content; MVD = median volume diameter of water droplet. The ice thickness is given for accretion zones (a) and (b) as defined in Figure 3.

The main characteristics of the ice accretion observed in the simulation are illustrated in Figure 2. The accretion process described in Koss *et al.* (2011) consists in essence of a continuous growth of the ice layer exhibiting different surface roughness and features in different characteristic accretion zones. Additionally, flow-out was observed for wet ice accretion. During the accretion process in the study the formation of distinct ice structures was observed significantly differing from layer-growth or flow-out as described above.

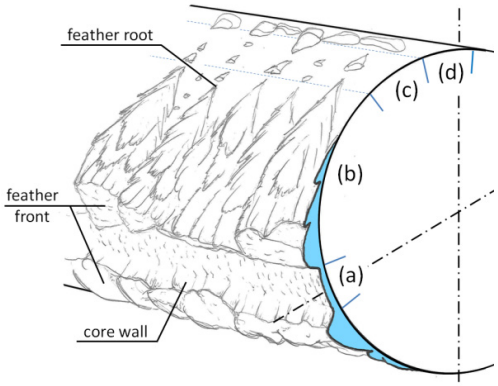


Main features of feather ice accretion with flow from the left and stagnation line in (a).

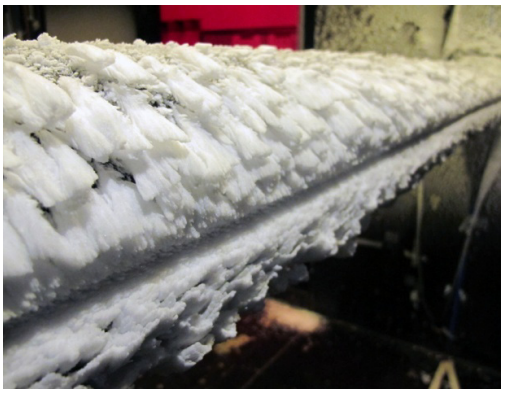

Feather ice accretion at -7.3°C air temperature and 5.8m/s airspeed after one hour (flow from the right).

Figure 2: Description of ice accretion characteristics as observed in the investigated cases.

With reference to Figure 2 and Koss *et al.* (2011) the accretion process can be summarised as follows: In the early stage of the process rime ice accumulates along the stagnation line quickly distinguishable as the smoother core zone (a) and boundaries of higher roughness. From the rougher boundary zones curved jagged ice structures start growing towards the stagnation line resembling the appearance of feathers until they reach a limit near the stagnation line, later constituting the core wall. More feather structures start growing from the outer accretion area (b). The growth rate is highest for new structures, slows down when aging and stops at the core wall. The starting point of the accretion (feather root) is affected by surface irregularities and climatic condition. Depending on temperature and *LWC* some flow-out (c) and flow-out accumulation (d) might occur. At temperatures below -4°C the feathers exhibit a fine jagged and highly detailed rime ice structure (hence *feather* resemblance) whereas liquid water at higher air temperature blunts the feathers and the accretion transforms into glaze ice. Here, excess water will lead to flow-out, rivulets or icicles near the separation line depending on cable orientation.

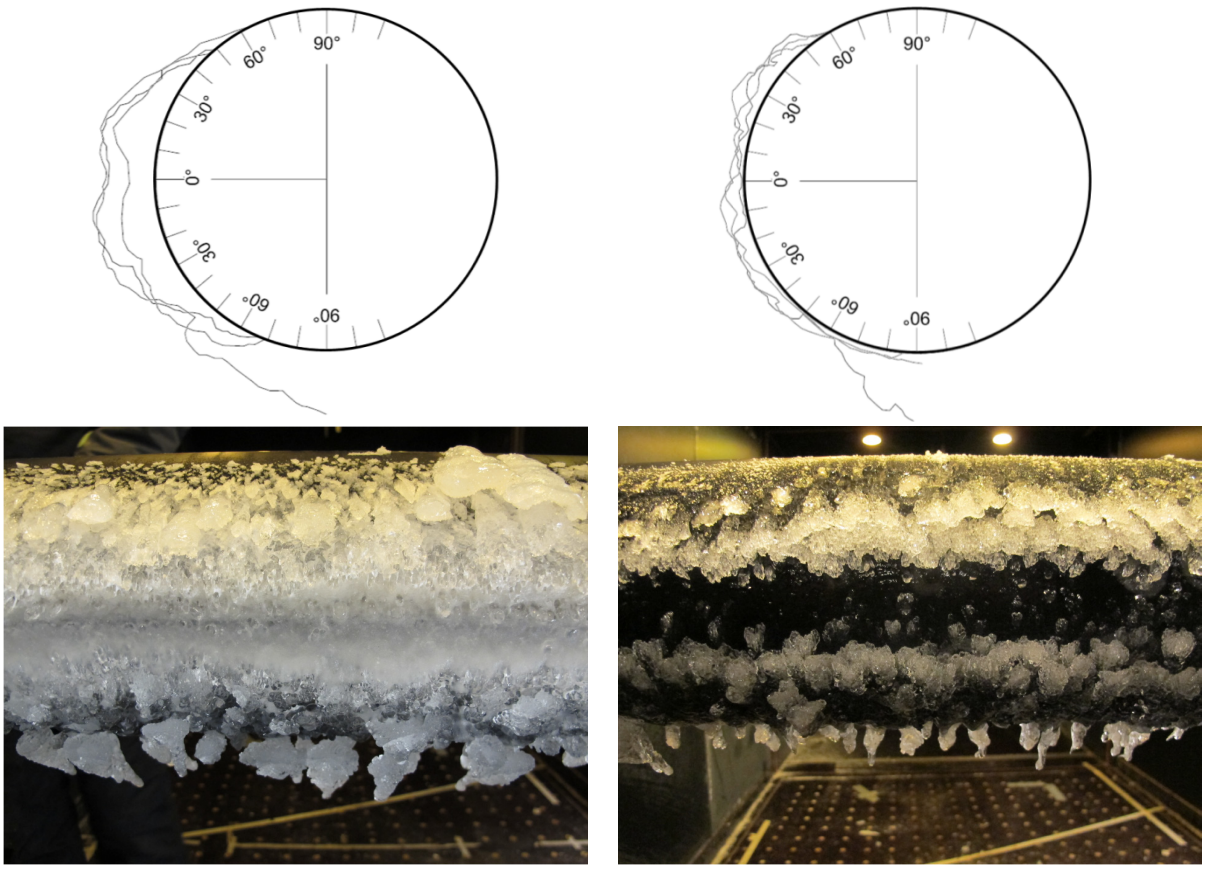


H1: airspeed 11m/s, air temperature -6.3°C H2: airspeed 11m/s, air temperature -3.2°C

Figure 3: Ice accretion after 60min. The contour lines (top of figure) were taken at three different positions of the cable to indicate the variation of the ice layer along the cable axis.

The contour lines and photographs in Figure 3 illustrate the ice accretion in the two cases considered in this study. Comparing photographs and contour lines demonstrates how little contour lines represent the complex shape of the ice accretion. This mismatch needs to be considered when studying ice effects on cable aerodynamics when using contour line moulding for ice layer models. Based on air temperature simulation H1 was expected to represent dry ice accretion but flow-out and icicle formation on the underside did occur presumable due to a significantly higher *LWC* than anticipated. Even though deviating from target settings the simulation is considered representing a likely condition of low-altitude atmospheric ice accretion.

## 4 Aerodynamic Load Coefficients

### *4.1 Definitions*

The forces acting on the cable section were measured on each side of the section with 6-component force balances (AMTI MC3A-500) as illustrated in Figure 4. When rotating the cable the force transducers followed the cable hence for flow-related forces ($F_D$, $F_L$) the measured signals ($F_x$, $F_y$) needed to be transformed. The moment was measured and analysed as well but the paper will discuss only drag and lift. The influence of temperature change on the force transducer (-15°C to +25°C) were tested in a special climate chamber at DTU and found to be negligible.

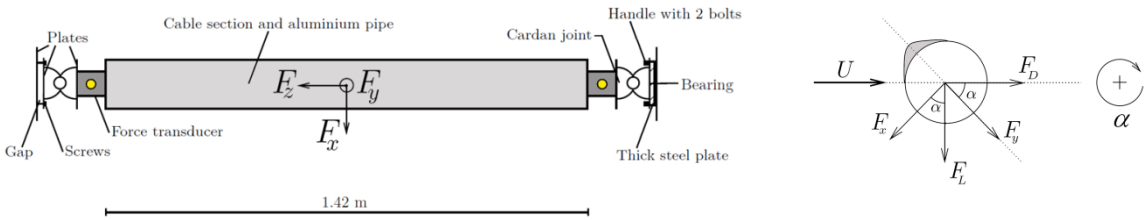


Force measurement arrangement (looking upstream) Force and rotation convention

Figure 4: Experimental setup and force convention for measuring the aerodynamic forces on the horizontal cable section. $\alpha$ is the positive direction of axial rotation.

## 4.2 Reference Drag and Lift

Using an original bridge cable cover tube section for the study the measured aerodynamic forces are affected by surface imperfections, roughness and by the cross-sectional ovality of the cable tube, which result from manufacturing process, storage, transport and installation (Matteoni and Georgakis, 2012). To evaluate the effect of icing on the aerodynamic forces the cable section was tested with dry surface as reference (Figure 5). The variations of drag and lift for different rotation angles $\alpha$ are very close to those found by Matteoni of Georgakis and are typical for this type of cover tube.

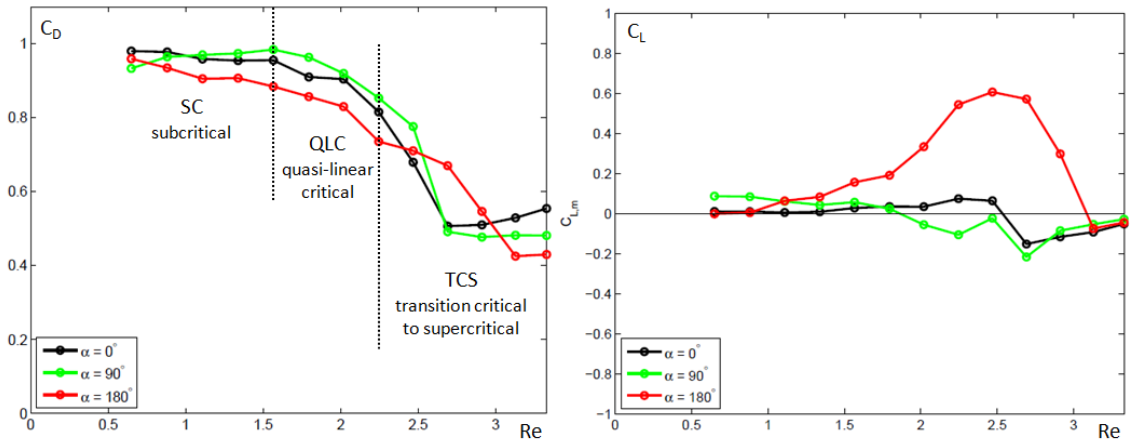


Figure 5: Drag ($C_D$) and lift ($C_L$) coefficient of the dry cable section for varying airspeed (Reynolds number) and different rotation angles α as reference. Along wind turbulence intensity $I_u$ = 0.6%.

For comparison with the results from iced cables the drag curve is divided into sub-ranges: subcritical (SC) where $C_D$ is nearly constant, a quasi-linear part of the critical range (QLC) and the transition from critical to supercritical (TCS) characterised by a high gradient of $C_D$ over Re-number.

## 4.3 H1: Drag and Lift

The drag and lift coefficients (Figure 6) depend on the angular position of the ice: high values for both occur where the ice is concentrated on the side of the cable. Furthermore, the location of the ice defines particular aerodynamic performance ranges: between $\alpha$ = 0° and 50° the drag coefficient varies with $\alpha$ but remains almost constant over the applied wind speeds, i.e. the effective shape exhibits subcritical behaviour (SC) throughout the applied Reynolds numbers. Between $\alpha$ = 50° and 130° $C_D$ varies nearly linear with *Re* hence reflecting a quasi linear behaviour (QLC). Beyond $\alpha$ = 130° the drag coefficients show a strong gradient over *Re*-number (TCS) as illustrated in Figure 5.

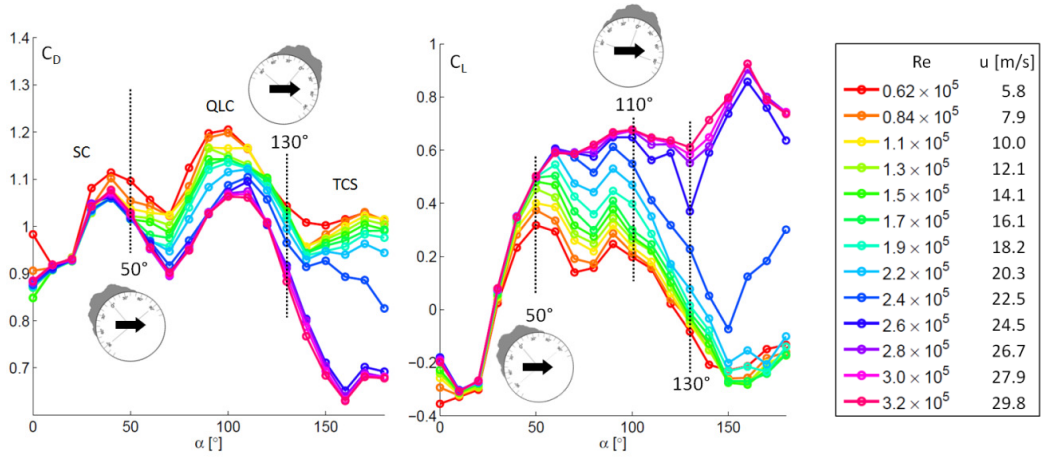


Figure 6: Drag and lift coefficient of the iced cable section in case H1 ($T_{air}$ = -6.3°C) for varying Reynolds number and different rotation angles α. Along wind turbulence intensity $I_u$ = 0.6%.

The dependency of $C_D$ on *Re* is a result of the ice layer influence on flow separation. A non-iced surface responds to *Re*-number whereas the ice layer provokes a sharp-edged bluff body behaviour less depending on *Re*. The performance ranges for lift are similar organised. Effective shapes for $\alpha$ beyond 130° show a high gradient of $C_L$ over *Re*.

### 4.4 H2: Drag and Lift

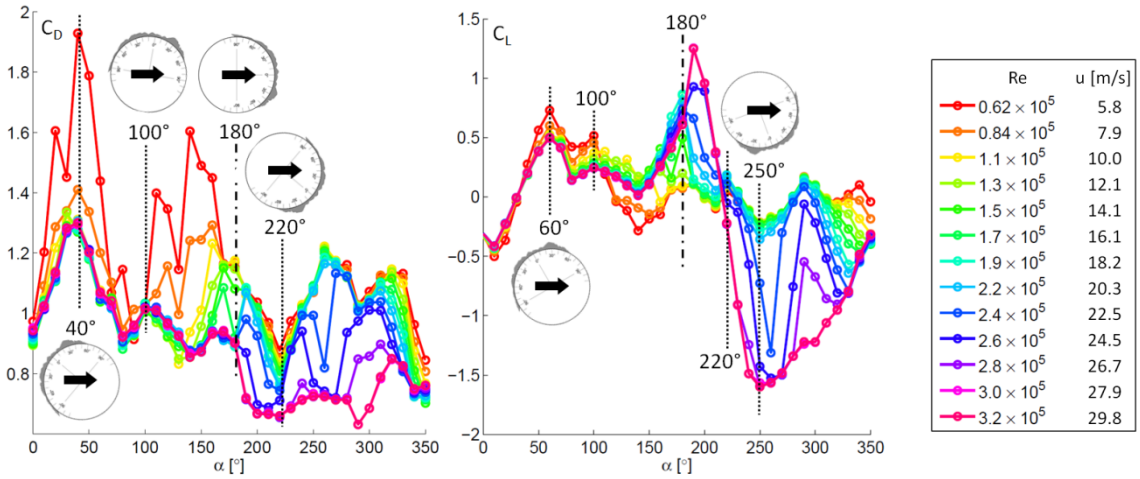


Figure 7: Drag and lift coefficient of the iced cable section in case H2 ($T_{air}$ = -3.8°C) for varying Reynolds number and different rotation angles α. Along wind turbulence intensity $I_u$ = 0.6%.

Apart from the lower two velocities the iced cable section reflects an invariance of the drag coefficient to *Re*-number up to a rotation angle of $\alpha$ = 150°. After a short transition the drag coefficient is beyond 180° characterised by a strong gradient within the tested velocity range (TCS). The lack of symmetry around 180° reflects the asymmetry of the ice layer quite likely due to the formation of larger pieces of ice on the underside of the cable section (Figure 3). The lift coefficient is as well affected by the asymmetry of the ice layer. A similar effect can be expected for case H1, which was for technical reasons only tested for incident flow directions between 0° and 180°.

## 5 Dynamic Response

The risk for aerodynamic instability is estimated from the galloping criterion formulated by Den Hartog (1958) using the measured drag and lift coefficients (Eqn. 1). Main condition for instability is the gradient of the lift coefficient $C_L(\alpha_c)$ over small changes in the incident flow direction $\alpha_c$ to the cable section.

$$H(\alpha) = \left( C_D(\alpha_c) - \frac{dC_L(\alpha_c)}{d\alpha_c} \right)\Bigg|_{\alpha_c=\alpha} \tag{1}$$

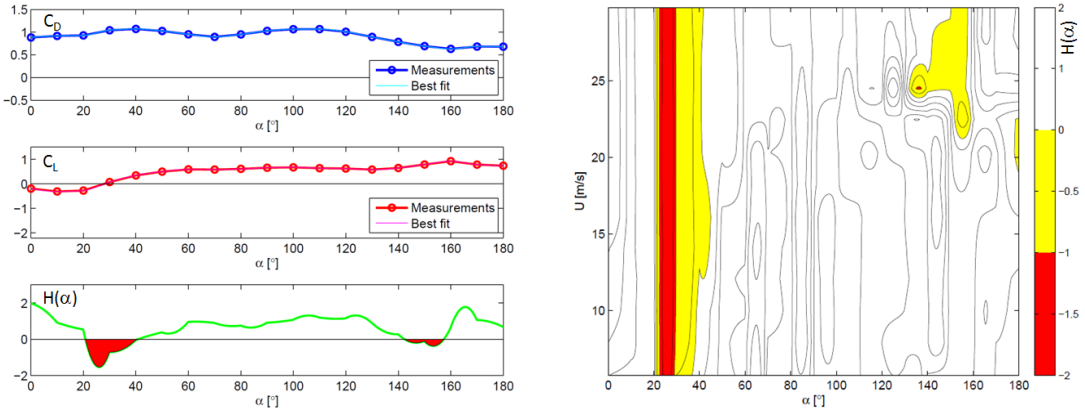


Figure 8: Case H1 - (*left*) example for evaluation of Den Hartog galloping criterion on force coefficients measured at U = 27.9m/s or Re = $3.5 \cdot 10^5$ respectively. (*right*) full evaluation of measurements from case H1.

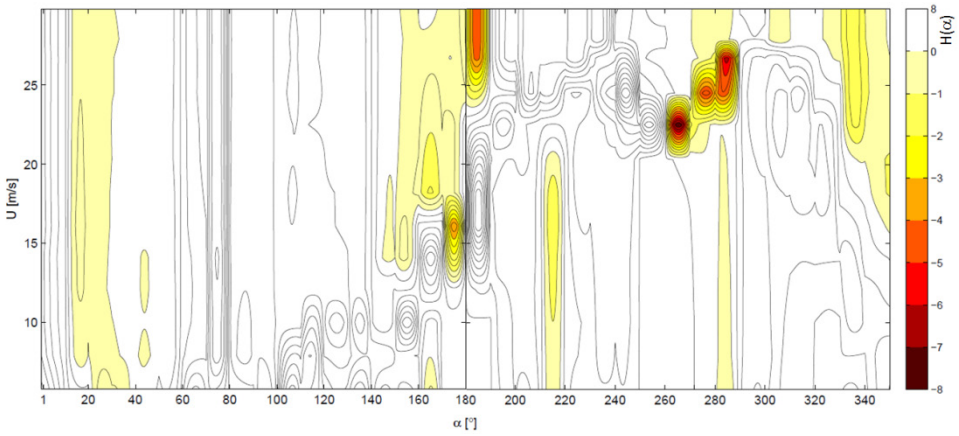


Figure 9: Full evaluation of Den Hartog criterion for Case H2.

Figures 8 and 9 show the evaluation of the Den Hartog criterion for both cases of ice accretion. The darker colours indicate the conditions where $H(\alpha)$ becomes negative, hence indicating a risk of galloping instability. In case H1 a strong indication of galloping is given for flow directions around 25° for all tested wind velocities and more isolated for 135° at 24.5m/s. Tests with an elastically suspended cable section with ice accretion confirmed instability for critical angular direction of $\alpha_c$ = 25° for wind speeds between $U$ = 15 and 29.8m/s. A second instability was found at $\alpha_c$ = 170° for wind speeds around 18.2m/s. Case H2 indicates in Figure 9 even more extreme conditions where galloping can be

expected. Repeating the icing of case H2 for dynamic response testing did not reflect any instability for the indicated conditions. This might be due to insufficient repeatability of the ice accretion.

## 6 Summary

The study shows the influence of low-altitude atmospheric icing on bridge cables on the aerodynamic forces for drag and lift. The extension of the ice layer influences the flow separation and hence the aerodynamic performance. This becomes in particular relevant when rotating the iced cable segment simulating a change of the wind direction after the icing incident. The effective body of the iced cable exhibits an aerodynamic drag behaviour reflecting only a part of the dry cable behaviour drag curve: either completely subcritical, i.e. constant $C_D$ for all tested *Re*-numbers, or quasi-linear drag drop over *Re* or a transition from critical to supercritical with a strong gradient of $C_D$ over *Re*. The lift coefficient exhibits similar characteristics. Testing the risk for galloping instability in a free vibration setup confirms some of predicted conditions but also some not indicated by the instability model. The dynamic testing suffers however from inaccuracy when repeating the ice accretion, which in future tests needs to be further explored.

## References

Demartino, C., Koss, H.H., Ricciardelli, F., 2013a. *Experimental study of the effect of icing on the aerodynamics of circular cylinders – Part I: Cross flow*. In: 6th European and African Conference on Wind Engineering, Cambridge, UK.

Demartino, C., Georgakis, C.T, Ricciardelli, F., 2013b. *Experimental study of the effect of icing on the aerodynamics of circular cylinders – Part II: Inclined flow*. In: 6th European and African Conference on Wind Engineering, Cambridge, UK.

Den Hartog, J.P., 1956. *Mechanical Vibrations*. 4th ed. McGraw-Hill, New York.

Fu, P., Farzaneh, M., Bouchard, G., 2006. *Two-dimensional modelling of the ice accretion process on transmission line wires and conductors.* Cold Regions Science and Technology, Vol.46 (2006), pp.132-146

Georgakis, C. T., Koss, H., Ricciardelli, F., 2009. *Design Specifications for a Novel Climatic Wind Tunnel for the Testing of Structural Cables*. Proceedings 8th International Symposium on Cable Dynamics, 2009, Paris, France

Gjelstrup, H., Larsen, A., Georgakis, C.T., Koss, H.H., 2008. *A new general 3-DOF quasi-steady aerodynamic instability model*. 6th International Colloquium on Bluff Bodies Aerodynamics and Applications, Milan, Italy, 2008

Koss, H., Gjelstrup, H., Georgakis, C.T., 2011. *Experimental study of ice accretion on circular cylinders at moderate low temperatures*. Proceedings 13th International Conference on Wind Engineering, Amsterdam, July 2011

Koss, H., Matteoni, G., 2011. *Experimental investigation of aerodynamic loads on iced cylinders*. Proceedings of 9th International Symposium on Cable Dynamics, Shanghai, October 2011

Matteoni, G., Georgakis, C.T., 2012. *Effect of bridge cable surface roughness and cross-sectional distortion on aerodynamic force coefficients*. Journal of Wind Engineering and Industrial Aerodynamics, Vol.104-106, May-July 2012, pp.176-187

Oleskiw, M.M., Hyde, F.H., Penna, J.P., 2001. *In-flight Icing Simulation Capabilities of NRC's Altitude Icing Wind Tunnel*. 39th AIAA Aerospace Science Meeting & Exhibit, January 2001, Reno, NV